Collective Thomson Scattering Measurement of Plasma Evolution During the Current Pulse in a Laser-Triggered Switch

Jacob A. Gottfried[1], Charles E. Rose[2], Sean Simpson[3], Azer P. Yalin[1*]

Affiliations

1: Department of Mechanical Engineering, Colorado State University, Fort Collins, CO. 80523, USA
2: Sandia National Laboratory, Albuquerque NM. 87123, USA
3: Zap Energy Inc, Seattle, WA, 98104, USA

*: Corresponding author: Azer.Yalin@colostate.edu

Abstract

High-voltage laser-triggered switches (HV-LTSs) are used in pulsed-power applications where low jitter and precise timing are required. The switches allow operation in the megaampere, megavolt regime while maintaining low insertion losses. Currently, there is a lack of detailed plasma measurements in these switches, yet such measurements are needed to elucidate the detailed physics which include a range of processes such as laser breakdown, streamer formation and growth, current flow, plasma evolution and cooling. Detailed spatially- and temporally- resolved measurements of plasma properties within the switches could contribute to validating and advancing numeric models of these systems. This contribution presents laser Thomson scattering measurements of the electron number density and temperature evolution in a HV-LTS. The switch was operated at 6 kV with current flow for duration of 145 ns and peak current density of 0.2 MA/cm^2 into a matched load. The Thomson scattering diagnostic system uses a 532 nm probe from an Nd:YAG laser allowing temporal resolution of ~10 ns. We find that during the switch current pulse, the plasma electron temperature rose from a starting value of 8.1±1.6 eV (due to cooling of the earlier trigger laser plasma) to a peak value of 26±5 eV, with an associated increase in electron density from 8.6 ±1.7x10^{17} cm^{-3} to 3.1±0.6x10^{18} cm^{-3}.

One of the earliest uses of lasers was for triggering of spark-gap switches to improve high-voltage switch performance[1–3]. Since then, laser-triggered spark-gap switches have become one of the main switching mechanisms for pulsed-power applications[4]. The popularity of these switches is largely due to their ability to deliver megampere (MA) currents and megavolt (MV) potentials in pulses of nanosecond to microsecond duration while maintaining low jitter on the order of picoseconds to nanoseconds[3–9]. Further, laser-triggering allows for the tight timing control necessary for large parallel MA class machines where many tens of High-Voltage Laser-Triggered Switches (HV-LTSs) are often utilized[10].

When used in laser-trigged mode, the switch electrodes are typically charged to a potential difference 15 – 25% below the self-breakdown voltage[4,6–12]. To trigger the switch, a high-energy laser pulse is focused between the switch electrodes causing the gas within the gap to breakdown and form a plasma kernel (spark)[3,4,11]. Due to the electric field from the electrodes, streamers emerge from the initial laser-induced spark until, after some delay, the plasma channel connects both electrodes, thus creating a highly conductive filament for current to flow[3–6].

The widespread use of laser-triggered spark-gap switches has driven numeric modeling of switch behavior (i.e., plasma channel formation, current flow through the switch, circuit descriptions of the switch etc.)[7,8,11,13–16]. The models in use today largely derive from the earlier works of Martin and Braginskii on the theory of (radial) growth of plasma channels. Phenomenologically, these models assume that during the rising edge (and plateauing) of the current flow through the switch, the switch plasma can be treated as a radially expanding cylinder with an attached blast wave that acts as a piston (and which detaches when the current flow decreases)[13,14]. The moving piston heats and ionizes the surrounding gas[13,14]. For the power-balance during the current-rise phase, it is assumed the effects of Joule heating within the plasma are canceled by the energy required for the shockwave and ionization, resulting in constant plasma conductivity (and in turn constant T_e)[6,9,13,14].

Recently developed low-inductance switches, designed for short pulse durations (order nanoseconds), where the transient rising and falling edges of the current dominate operation, have revealed discrepancies between simulated and experimental behavior[7]. Continued validation and development of models for HV-LTSs is limited by the current lack of detailed *in situ* plasma measurements, particularly during the critical rising-edge of the current pulse (where the authors are aware of no reported plasma data).

The goal of the present contribution is to develop an experimental diagnostic system utilizing laser Thomson scattering to measure the temporal profiles of electron temperature (T_e) and density (n_e) of the plasma channel within a HV-LTS, with emphasis on capturing the behavior during the rising edge of the current pulse. Laser Thomson scattering was originally developed for nuclear fusion applications in the 1960s[17]. Since then, Thomson scattering has been applied over a broad range of both electron temperature (~0.1–10 eV) and density (~10^{13}-10^{20} cm^{-3})[9,18–24] and pulse rates up to 10 kHz[25]. The Thomson diagnostic setup described here is oriented to conditions in the HV-LTS switch, i.e., T_e ~10–30 eV and n_e ~ 10^{17} -10^{18} cm^{-3}.

For experimentation at relevant conditions, we have developed a testbed based on

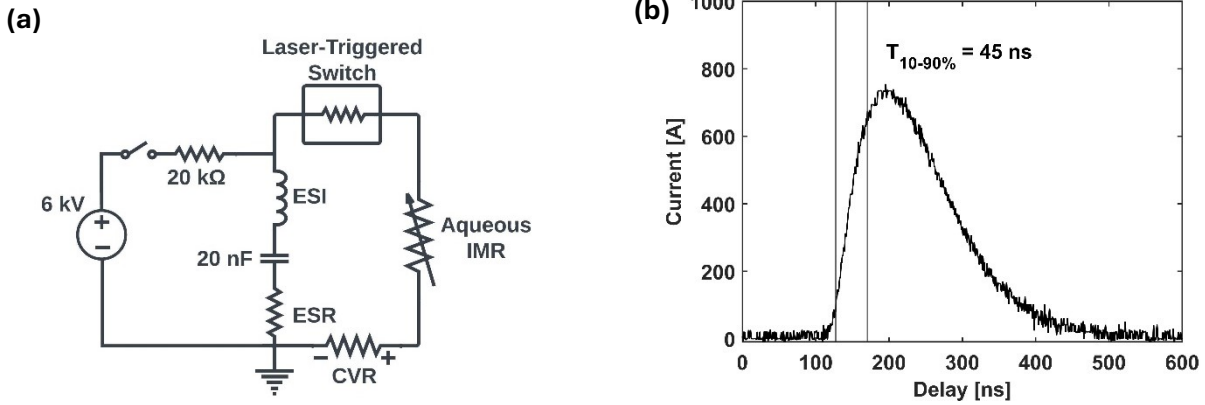

Figure 1 A) Electrical circuit of HV-LTS where ESI and ESR are the equivalent series inductance (~200 nH) and resistance, and IMR is impedance matching resistor (~6 Ω) B) Experimental current trace from the current viewing resistor for 6 kV switch operation.

a laser-triggered 3.5 mm spark-gap switch with optical access for diagnostics[6,9,11]. Measurements use atmospheric pressure zero air as the switch working gas. Figure 1a depicts the electrical circuit of the switch. Energy storage is provided by a 20 nF, 100 kV capacitor and a low overall circuit inductance ~200 nH. Charge energy is provided by a 125 kV DC power supply through a 20 kΩ liquid charge/isolation resistor. (The HV-LTS can operate up to maximum voltage of 200 kV.) Once the capacitor is charged to the desired voltage, a relay electrically isolates the switch prior to triggering. Circuit current is measured by an integral current viewing resistor (CVR, T&M Research Products W-2-001-6FC).

A variable aqueous impedance matching resistor (IMR) is used to both simulate a realistic pulsed-power load[26–29] and provide impedance matching to minimize reflections. The IMR was designed to use a simple sodium chloride/distilled water solution with a load water processing loop allowing for fine control of solution concentration necessary for load matching *in situ.* The resistance (of switch plus surrounding circuit to load) is tuned such that reflections have been minimized and are undetectable with our setup. For the 6 kV charge condition used in this letter, the matched resistance is ~6 Ω.

Figure 1b is experimental data of circuit current as seen by the CVR and recorded by an oscilloscope (Tektronix TDS5034B). This profile shows switch closure at ~120 ns after the trigger laser pulse with jitter of ±7 ns (based on extrema of replicate measurements). The current-pulse duration full-width-half-maximum (FWHM) is 145 ns with a peak of ~735 A and 10-90% rise-time of 45 ns.

Figure 2 shows the overall optical setup including the triggering laser and Thomson scattering diagnostics. Laser-triggering of the switch is by the 1064 nm output of an Nd:YAG laser (Quantel Big Sky) with pulse energy of 14 mJ and pulse duration of 12 ns. The beam has a collimated diameter of ~3 mm and is focused by a short focal length (f=18 mm; L_2) lens to a relatively tight waist that is positioned (~±0.5 mm) at the center between electrodes. The focused optical intensity of the trigger laser is above the breakdown threshold such that a laser-induced plasma is formed with an initial kernel at the beam waist.

In the axial direction, the laser plasma kernel is smaller than the electrode separation (i.e., the plasma forms in the gas only and not on the electrodes). The evolution of the plasma channel diameter is determined by imaging the visible luminosity with a full-chip ICCD

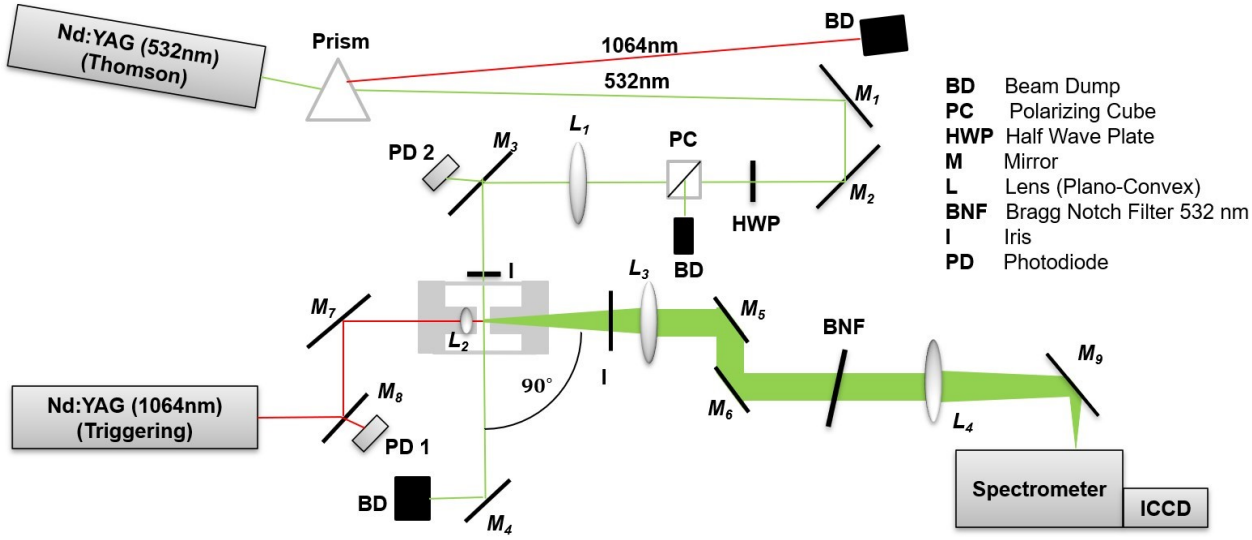

Figure 2. Optical setup for laser Thomson scattering diagnostic and laser triggering of switch.

(Princeton Instruments PI-MAX4:1024f). A thresholding technique is used to find the contour of the plasma from images at different times. The plasma channel diameter is observed to expand from ~0.5 mm to ~1.2 mm during the current pulse. After the current pulse, from time ~400 ns to ~2 μs (relative to laser trigger), the plasma channel diameter continues to grow at a rate of $t\hat{}(0.63 \pm 0.017)$, based on fitting the imaging data. This power-law dependence is similar to what has been reported for other spark gap switches[5,6,14]. A peak current density of 0.21 MA/cm^2 is recorded when the plasma channel diameter is 0.65 mm.

The Thomson scattering measurements use a frequency-doubled Nd:YAG (Quantel Q-Smart 100) operating at 532 nm with a pulse energy of 28 mJ and duration 8 ns. A half-waveplate and polarizer are used to control the beam energy and set a linear polarization perpendicular to the plane of the scattering. (This polarization maximizes the Thomson signal while avoiding plasma heating from a polarization component that does not contribute to the Thomson signal.) The Thomson beam is weakly focused with a 400 mm focal length lens (L_1) positioned such that the focal point is at an iris just upstream of the switch. At the location of the plasma channel, the probe beam diameter is ~0.9 mm. The Thomson probe beam fluence at the measurement location is ~1.1 J/cm^2, several orders of magnitudes lower than what is typically used for laser Thomson scattering[23,24,30–34]. The low fluence is used to minimize heating of the plasma by the probe beam through inverse-Bremsstrahlung absorption[35].

The scattered light, along with plasma luminous emission, is collected and collimated by a lens (L_3) through an iris set to 1 cm. The iris limits the collection solid-angle leading to improved performance of the Bragg Notch Filter (BNF) that is designed for collimated incident light. The BNF provides an optical density of ~3 for the 532 nm laser-line with FWHM of 0.1 nm. The role of the BNF is to suppress the Rayleigh and elastically scattered laser light from saturating the ICCD and/or distorting the recorded spectra. The collected light is imaged onto the 40 μm width slit of a monochromator (Princeton Instruments SP-2300i) using 1:1 magnification relative to the probe volume. The light is dispersed with a 1200 groove/mm grating onto the ICCD using a gate width of 10 ns. The resulting spectral resolution and wavelength range are 0.030 and 30 nm respectively.

We report temporally resolved plasma measurements based on delay between the measurement time (defined as the center of probe laser) and the laser trigger time (defined as the 10% rise in signal of photodiode PD1). A delay generator (Stanford Research Instruments DG535) is used to set the laser pulse timings.

To determine electron density and temperature from experimental Thomson spectra, the data are fit with a simulation. For the electron properties in this letter, the scattering parameter, α, which describes the nature of the Thomson scattering, is in the range of 2-4, the collective regime[23,24,36–38]. The scattering parameter is defined as[38]:

$$\alpha \equiv \sqrt{\frac{n_e e^2}{T_e k_B \varepsilon_0 k^2}} = \frac{1}{k\lambda_D} \qquad (1)$$

where k_B is the Boltzmann constant, ε_0 is the vacuum permittivity of free space, k is the wavenumber of the incident light and λ_D is the Debye radius of the plasma.

In collective Thomson scattering, scattering takes place over an optical wavelength greater than the Debye radius of the plasma, and therefore interactions are with shielded electrons. During the interactions, the photons are accelerated by charged particles in the plasma[9,20,23,37,39]. In the case of collective-Thomson scattering, the Doppler shifted photons result in two satellite peaks in the spectrum that are symmetrically shifted from the laser's incident wavelength[23,30,31,39]. In addition to the electron features, there is also a ionic feature, however, the large mass of the ions results in this feature being spectrally close to the incident

laser's wavelength[23]. We do not consider the ion feature in this letter.

Assuming the electron energy distribution function (EEDF) is Maxwellian[21,23,40], the Salpeter approximation of the scattering form factor, $S(\boldsymbol{k},\omega)$, is used[38,41]:

$$S(\boldsymbol{k},\omega) \approx \frac{\sqrt{2\pi}}{\nu_{te}}\Gamma_{\alpha}(\xi_e) \quad (2)$$

where the line shape function, Γ_{α}, is:

$$\Gamma_{\alpha}(\xi_e) = \frac{\exp\left(-{\xi_e}^2\right)}{|1+\alpha^2 w(\xi_e)|^2} \quad (3)$$

where the plasma dispersion function, $w(\xi_e)$, is[42]:

$$w(\xi_e) = 1 - 2\xi_e e^{-{\xi_e}^2}\int_0^{\xi_e} e^{-\zeta^2}d\zeta + i\pi^{\frac{1}{2}}\xi_e e^{-{\xi_e}^2} \quad (4)$$

where the ratio, ξ_e, of wave phase velocity to the electron thermal velocity is[42]:

$$\xi_e = \frac{\omega}{k\nu_{te}\sqrt{2}} \quad (5)$$

and the electron thermal velocity, $\nu_{te,}$ is:

$$\nu_{te} = \sqrt{\frac{8k_B T_e}{\pi m_e}} \quad (6)$$

Therefore, the scattering form factor is a function of T_e, allowing for the electron temperature to be determined from measured LTS spectra. In addition to electron temperature, the electron density can also be determined from the wavelength separation of the (electron) satellite peaks from the incident laser wavelength[23]:

$$\Delta\omega_e = \pm\left(\omega_{pl}^2 + \frac{3k_B T_e k^2}{m_e}\right)^{\frac{1}{2}} \quad (7)$$

where the plasma frequency, ω_{pl} is:

$$\omega_{pl} = \sqrt{\frac{e^2 n_e}{\varepsilon_o m_e}} \quad (8)$$

The above equations allow computation of a synthetic Thomson scattering spectrum based on assumed values of electron temperature and density. To further improve simulation accuracy, a calibration is performed with Rotational Raman Scattering[9]. Best-fit values of n_e and T_e are based on seeking the best agreement (via least-squares minimization) between a measured spectrum and simulated spectra. Figure 3 shows an example of a simulated Thomson fit with corresponding experimental data (each data point is a 200 shot average). The plotted spectra are after subtracting the plasma background (which is collected under the same conditions as the Thomson measurement but without the probe beam). At delay times less than 340 ns, the simulation and fit were only performed on a single peak[30]. This method was used due to the wavelength separation of the satellite peaks being greater than the wavelength range of a single ICCD image.

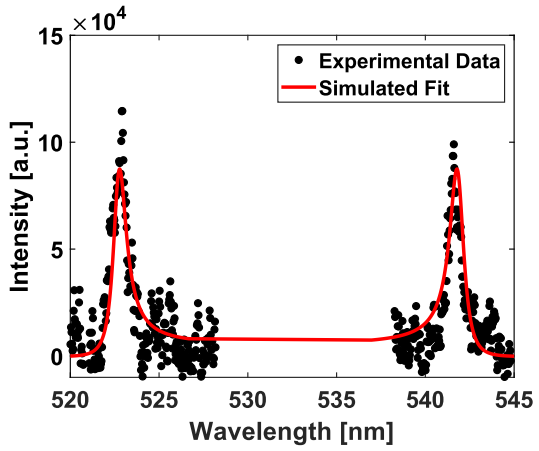

Figure 3 Simulated Thomson scattering fit of experimental data for delay of 450 ns yielding T_e= 8.1±1.6 eV and n_e=7.3±1.5x10^{17} cm^{-3}.

Thomson scattering has a small cross-section resulting in a low scattering power relative to the plasma luminosity[20]. Therefore, at each measurement condition, 200 Thomson spectra (switch firings) were recorded and averaged to achieve sufficient signal-to-noise. Another challenge is that at most measurement conditions, the Thomson satellite peaks are overlapped by N II ionic emission lines between ~545–560 nm[43]. To minimize the impact of the rapidly changing emission on the Thomson spectra (even after background subtraction), it is essential to use short ICCD time-gate windows[44,45]. In many cases, the optical emission is as much as 100 times stronger than the Thomson peaks, reinforcing the need to subtract

a plasma background spectrum. The above factors limit the signal-to-noise ratio and dominate the final uncertainty which is found as ~±20% for both electron density and temperature based on the combination of standard-deviation of repeat measurements and error in fitting simulations to experimental data. The uncertainty on reported delay time is ±10 ns due to combined contributions of equipment timing jitter.

Figure 4 shows the measured electron temperature, plotted versus delay (relative to laser trigger), during the current flow through the switch. These data are overlaid with the current profile measured by the CVR. The profile can be considered in three temporal regimes based on switch current flow: A) before current-flow (delay $\lesssim$120 ns), B) increasing current flow (delay ~120–200 ns), C) decaying current flow (delay $\gtrsim$ 200 ns).

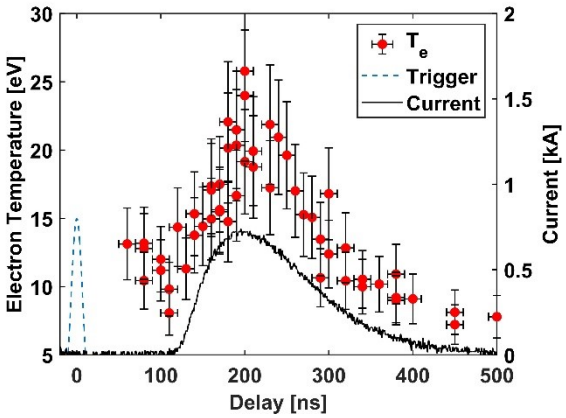

Figure 4 Electron temperature during current pulse of HV-LTS operating at 6 kV. Trigger refers to the time of the triggering laser pulse.

In the first phase, before ~120 ns, the switch has not closed and only the plasma produced by the trigger laser is present. This laser induced plasma has an initial peak temperature and density (defined by the energy deposition of the trigger laser) which then decay, as would occur in the absence of the switch, until the time of switch closure (current flow).

The second region commences at the time of switch closure, i.e., onset of current flow, at ~120 ns, and continues until the current maximizes at ~200 ns. Importantly, and in contrast to the assumptions of Martin and Braginskii, Thomson measurements reveal increasing T_e during this phase. At the start of the rising-edge of the current flow, the plasma temperature is ~8.1±1.6 eV (as defined by the cooling of the trigger laser plasma and consistent with measurements of similar laser-induced air plasmas[23]). The electron temperature continues to increase until a maximum of ~26±5 eV is reached at delay 200 ns, which closely matches the time of the maximum recorded current. The rise in temperature during the current flow is likely due to Joule heating. The electron temperature is proportional to the DC plasma conductivity[46] and therefore plays an essential part in modeling the electrical characteristics of the plasma channel. There is currently no published experimental data on the evolution of the electron temperature during the rising-edge of the current-pulse. Furthermore, this represents empirical data showing a breakdown of a key assumption (constant T_e during current rise) in the Martin/Braginskii HV-LTS model, indicating that our switch is likely not well described by that model.

The final temporal section is after 200 ns and corresponds to the falling edge of the current pulse. During the falling edge, we find that the electron temperature decays at a rate proportional to $t^{-1.48}$. A similar rate of decay continues for ~1.5 microseconds following the end of the current pulse.

Figure 5 is a plot of the evolution of electron density and can also be interpreted based on the same three temporal regimes. Before the switch closes at ~120 ns, the electron density of the laser-induced plasma is 8.6±1.8x10^{17} cm^{-3} (also comparable to values for similar laser induced plasmas[23]).

During the rising edge of the current, ~120 – 200 ns, there is a rapid increase in electron density to a maximum value of ~3.1±0.6x10^{18} cm^{-3}. The maximum electron density represents an ionization fraction of ~0.12 of the ambient air

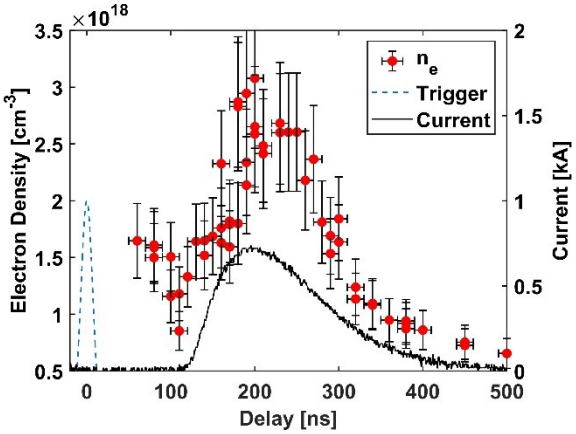

Figure 5 Electron density during current pulse of HV-LTS operating at 6 kV. Trigger refers to the time of the triggering laser pulse.

within the switch (assuming singly-charged ions). An important note about the electron density rise during the time of current flow is the current flowing through the plasma channel cannot directly account for it. This conclusion is based on finding that the peak electron density due to the current is $\lesssim$10% of the peak electron density measured from Thomson scattering. The former is estimated by temporally-integrating the current signal and dividing it by the approximate plasma volume while the latter comes directly from Thomson measurements (after subtracting the electron contribution from the decay of the trigger pulse). It is believed the rise in electron density during current flow is due to Joule heating in the plasma (and surrounding gas) leading to an increase in ionization.

During the falling edge of the current pulse there is an initial rapid decrease in electron density for the first tens of nanoseconds which is then followed by a relatively constant power-law decay of $\sim t^{-1.64}$ that lasts for several microseconds after the current pulse. These results qualitatively match simulated results for a laser-triggered plasma channel in air where it was found that, following ionization, there is an initial rapid decline in electron density due to recombination followed by a slower loss of electrons due to attachment[47].

In conclusion, this letter demonstrates the viability of an experimental and diagnostic testbed to measure the evolution of electron properties during current flow within a HV-LTS. The measurements provide nanosecond temporally resolved measurements of electron temperature during a current pulse through a plasma channel. During the critical rising-edge portion of the current flow, we observe an increase in electron temperature caused by Joule heating and an increase in electron density due to increased ionization. The increase in T_e during this regime is at odds with the assumption of constant T_e used in some switch models emphasizing the need to consider underlying assumptions when selecting suitable models for a given switch.

Future work will include spatially resolved study of the plasma properties (by using the spatial axis of the ICCD which corresponds to ~13 μm per pixel in the current setup) as well as studying the plasma and switch closure for different fill gases at different pressures. While synthetic air is a common working gas in these switches, other gases such as noble gases and SF_6 are also used.

Acknowledgments

Colorado State University acknowledges funding support from Sandia National Laboratories. Sandia National Laboratories is a multi-mission laboratory managed and operated by National Technology & Engineering Solutions of Sandia, LLC, a wholly owned subsidiary of Honeywell International, Inc., for the U.S. Department of Energy's National Nuclear Security Administration under contract DE-NA0003525.

This paper describes objective technical results and analysis. Any subjective views or opinions that might be expressed in the paper do not necessarily represent the views of the U.S. Department of Energy or the United States Government.

We would also like to acknowledge funding support from the National Science Foundation Division of Physics Award 2010466.

Authors Declarations

Conflicts of Interest

The authors have no conflicts to disclose.

Author Contributions

Jacob A. Gottfried: Formal Analysis (lead); Investigation (equal); Writing/Original Draft Preparation (lead); Writing/Review & Editing (equal); Conceptualization (support); Methodology (equal). **Charles E. Rose:** Writing/Review & Editing (support); Conceptualization (support). **Sean Simpson**: Writing/Review & Editing (support); Conceptualization (support). **Azer P. Yalin:** Supervision (lead); Writing/Review & Editing (equal); Conceptualization (lead); Methodology (equal) Formal Analysis (support).

DATA AVAILABILITY

The data that support the findings of this study are available from the corresponding author upon reasonable request.

References

[1] W.K. Pendleton and A.H. Guenther, Review of Scientific Instruments **36**, 1546 (1965).
[2] A. Guenther and J. Bettis, IEEE J. Quantum Electron. **3**, 581 (1967).
[3] A.H. Guenther and J.R. Bettis, J. Phys. D: Appl. Phys. **11**, 1577 (1978).
[4] A. Larsson, D. Yap, J. Au, and T.E. Carlsson, IEEE Trans. Plasma Sci. **42**, 2943 (2014).
[5] M.F. Wolford, M.C. Myers, F. Hegeler, and J.D. Sethian, IEEE Trans. Plasma Sci. **44**, 2410 (2016).
[6] C.E. Rose, M.Sc. Thesis, Mechanical Engineering Dept., Colorado State University, Fort Collins, CO 69 (2019).
[7] S. Simpson, O. Johns, C. Rose, J. Leckbee, C. Dumitrache, D. Nielsen, A. Yalin, and M. Kiefer, IEEE Pulsed Power Conference **Brighton, United Kingdom**, 25 (2017).
[8] D.R. Welch, D.V. Rose, C. Thoma, R.E. Clark, C. Miller, E.A. Madrid, W.R. Zimmerman, P.K. Rambo, J. Schwarz, M. Savage, and B.W. Atherton, Physics of Plasmas **20**, 083108 (2013).
[9] J.A. Gottfried, M. Roux, and A.P. Yalin, AIAA Aviation 2022 Forum 14 (2022).
[10] K. LeChien, M. Savage, V. Anaya, D. Bliss, W. Clark, J. Corley, G. Feltz, J. Garrity, D. Guthrie, K. Hodge, J. Maenchen, R. Maier, K. Prestwich, K. Struve, W. Stygar, T. Thompson, J. Van Den Avyle, P. Wakeland, Z. Wallace, and J. Woodworth, Phys. Rev. ST Accel. Beams **11**, 060402 (2008).
[11] C. Rose, S.G. Patel, S. Simpson, and A.P. Yalin, in *AIAA Aviation 2019 Forum* (American Institute of Aeronautics and Astronautics, Dallas, Texas, 2019).
[12] Y. Raizer, *Gas Discharge Physics*, 1st ed. (Springer Berlin, Heidelberg, 1991).
[13] S. Braginskii, J. Exptl. Throret. Phys. **34**, (1958).
[14] T.H. Martin, J.F. Seamen, and D.O. Jobe, in *Ninth IEEE International Pulsed Power Conference* (IEEE, Albuquerque, NM, USA, 1993), p. 463.
[15] R. Montano, M. Becerra, V. Cooray, M. Rahman, and P. Liyanage, IEEE Trans. Plasma Sci. **34**, 1610 (2006).
[16] M.J. Kushner, W.D. Kimura, and S.R. Byron, Journal of Applied Physics **58**, 1744 (1985).
[17] N.J. Peacock, D.C. Robinson, M.J. Forrest, P.D. Wilcock, and V.V. Sannikov, Nature **224**, 488 (1969).
[18] K. Uchino, T. Muraoka, K. Muraoka, and M. Akazaki, Jpn. J. Appl. Phys. **21**, L696 (1982).
[19] K. Uchino, Y. Itsumi, K. Muraoka, and M. Akazaki, Jpn. J. Appl. Phys. **23**, 662 (1984).
[20] K. Muraoka and A. Kono, J. Phys. D: Appl. Phys. **44**, 043001 (2011).
[21] C.S. Murray, M.Sc. Thesis, Physics Dept., Wright State University, Dayton, OH 68 (2020).
[22] A.J. Friss, Ph.D. Dissertation, Mechanical Engineering Dept., Colorado State University, Fort Collins, CO 183 (2019).
[23] K. Dzierże˛ga, A. Mendys, and B. Pokrzywka, Spectrochimica Acta Part B: Atomic Spectroscopy **98**, 76 (2014).

[24] B. Vincent, S. Tsikata, S. Mazouffre, T. Minea, and J. Fils, Plasma Sources Sci. Technol. **27**, 055002 (2018).
[25] Z. He, C. Smith, Z. Zhang, T.M. Biewer, N. Jiang, P.S. Hsu, and S. Roy, Plasma Sci. Technol. **21**, 105603 (2019).
[26] R.E. Beverly and R.N. Campbell, Review of Scientific Instruments **66**, 5625 (1995).
[27] N. Gavish and K. Promislow, Phys. Rev. E **94**, 012611 (2016).
[28] R.V. Whiteley and J.M. Wilson, 4 (n.d.).
[29] J.B. Hasted, D.M. Ritson, and C.H. Collie, The Journal of Chemical Physics **16**, 1 (1948).
[30] K. Dzierżęga, A. Mendys, S. Pellerin, E. Thouin, G. Travaille, B. Bousquet, L. Canioni, and B. Pokrzywka, (2010).
[31] K. Tomita, T. Kagawa, K. Uchino, S. Katsuki, and H. Akiyama, 5 (2009).
[32] T. Hatae, A. Nagashima, T. Kondoh, S. Kitamura, T. Kashiwabara, H. Yoshida, O. Naito, K. Shimizu, O. Yamashita, and T. Sakuma, Review of Scientific Instruments **70**, 772 (1999).
[33] Y. Sato, K. Tomita, S. Tsukiyama, T. Eguchi, K. Uchino, K. Kouge, H. Tomuro, T. Yanagida, Y. Wada, M. Kunishima, T. Kodama, and H. Mizoguchi, Jpn. J. Appl. Phys. **56**, 036201 (2017).
[34] A. Mendys, M. Kański, A. Farah-Sougueh, S. Pellerin, B. Pokrzywka, and K. Dzierżęga, Spectrochimica Acta Part B: Atomic Spectroscopy **96**, 61 (2014).
[35] G. Travaillé, A. Mendys, K. Dzierzega, S. Pellerin, B. Pokrzywka, E. Thouin, B. Bousquet, and L. Canioni, Contrib. Plasma Phys. **51**, 171 (2011).
[36] K. Warner and G.M. Hieftje, Spectrochimica Acta Part B: Atomic Spectroscopy **57**, 201 (2002).
[37] J.S. Ross, S.H. Glenzer, J.P. Palastro, B.B. Pollock, D. Price, G.R. Tynan, and D.H. Froula, Review of Scientific Instruments **81**, 10D523 (2010).
[38] E.E. Salpeter, Physical Review **120**, 1528 (1960).
[39] M. van de Sande and M.J. van de Sande, *Laser Scattering on Low Temperature Plasmas: High Resolution and Stray Light Rejection* (2002).
[40] M. Huang, P.Y. Yang, D.S. Hanselman, C.A. Monnig, and G.M. Hieftje, Spectrochimica Acta Part B: Atomic Spectroscopy **45**, 511 (1990).
[41] I.H. Hutchinson, *Principles of Plasma Diagnostics*, Second (Cambridge University Press, 2002).
[42] B.D. Fried and S.D. Conte, in *The Plasma Dispersion Function* (Elsevier, 1961), pp. 5–7.
[43] H. El-Rabii, S.B. Victorov, and A.P. Yalin, J. Phys. D: Appl. Phys. **42**, 075203 (2009).
[44] W.A. Cilliers, J.D. Hey, and J.P.S. Rash, Journal of Quantitative Spectroscopy and Radiative Transfer **15**, 963 (1975).
[45] G. Cristoforetti, A. De Giacomo, M. Dell'Aglio, S. Legnaioli, E. Tognoni, V. Palleschi, and N. Omenetto, Spectrochimica Acta Part B: Atomic Spectroscopy **65**, 86 (2010).
[46] M.A. Lieberman and A. Lichtenberg, *Principles of Plasma Discharges and Materials Processing* (John Wiley & Sons, 2005).
[47] Tz.B. Petrova, H.D. Ladouceur, and A.P. Baronavski, Physics of Plasmas **15**, 053501 (2008).